

Banner appropriate to article type will appear here in typeset article

# The effect of local ventilation on airborne viral transmission in indoor spaces

Alexander Pretty<sup>1</sup>†, Ian M. Griffiths<sup>2</sup>, Zechariah Lau<sup>1,2</sup> and Katerina Kaouri<sup>1</sup>

<sup>1</sup>School of Mathematics, Cardiff University, Cardiff, CF24 4AG, UK

<sup>2</sup>Mathematical Institute, University of Oxford, Oxford, OX2 6GG, UK

(Received xx; revised xx; accepted xx)

We incorporate local ventilation effects into a spatially dependent generalisation of the Wells–Riley model of airborne viral transmission. Aerosol production and removal through ventilation (global and local), biological deactivation, and gravitational settling as well as transport around a recirculating air-conditioning flow and turbulent mixing are modelled using an advection–diffusion–reaction equation. The local ventilation effects are compared with the equivalent global ventilation and we find that the streamlines of the airflow provide insight into when the global ventilation model is a good approximation. When the agreement between ventilation models is poor, we find that the global ventilation model generally overestimates the infection risk.

**Key words:**

---

## 1. Introduction

The importance of ventilation in reducing the indoor transmission of infectious diseases was first highlighted by Nightingale (1860). When an infectious person breathes, talks, coughs, or sneezes, disease-carrying particles are emitted. In poorly ventilated spaces, small particles known as *aerosols* can remain airborne for several hours, transmitting the disease to susceptible people when inhaled. During the COVID-19 pandemic, a key shift in understanding and mitigating transmission of the SARS-CoV-2 virus was the recognition of airborne transmission (Morawska & Milton 2020), most likely responsible for superspreader outbreaks in a restaurant (Ho 2021), courtroom (Vernez *et al.* 2021), choir practice (Miller 2021), and meat processing plant (Günther 2020).

There are two main approaches to modelling airborne transmission: Wells–Riley models and Computational Fluid Dynamics (CFD). Wells–Riley models (Riley *et al.* 1978) assume a well-mixed-room (WMR), meaning aerosols are instantaneously transported throughout the room. Due to its high computational speed, this approach can be readily applied at the start of an epidemic. This was the case for COVID-19 (Buonanno *et al.* 2020; Dai & Zhao

† Email address for correspondence: prettya@cardiff.ac.uk

2020; Lelieveld 2020). However, the WMR assumption is not always appropriate and cannot provide any information on the spatial variation of the concentration.

CFD models simulate the (usually turbulent) airflow in a room. The computational demand is high, so many CFD studies at the start of the COVID-19 pandemic focused on relatively short time frames (less than 5 minutes) (Shafaghi *et al.* 2020; Vuorinen 2020) whereas airborne transmission typically occurs over hours. Some CFD models have simulated aerosol evolution for up to an hour (Shao *et al.* 2021), but the high computational times means that CFD can not easily inform up-to-date decisions in a quickly developing epidemic.

Lau *et al.* (2022) model the spatiotemporal evolution of aerosols in a room using an advection–diffusion–reaction (ADR) equation under the assumption of a recirculating airflow. Unlike Wells–Riley models, the ADR model accounts for the spatial variation of concentration and infection risk. Moreover, the simplified 2D airflow allows fast simulations so the ADR model can be quickly deployed in a fast-changing epidemic. In Lau *et al.* (2022), aerosol removal by ventilation is modelled as a global sink, as in the Wells–Riley type models. This assumption produces good agreement with real-life scenarios ventilated by inbuilt air-conditioning (AC) units (Lau *et al.* 2022).

For rooms with poor or non-existent AC, air purifiers can increase overall aerosol removal. The effectiveness of air purifiers depends strongly on their location (Burgmann & Janoske 2021; Narayanan & Yang 2021), an effect that cannot be captured by the WMR assumption or the global sink of Lau *et al.* (2022). Moreover, many CFD studies of air purifiers report prohibitively long computational times; for example Dbouk *et al.* (2021) report 7 days to simulate a 2.5 minute event in a domestic setting. While air purifiers are not technically classified as ventilation, since they do not provide fresh air from outdoors, the American Society of Heating, Refrigeration and Air-Conditioning (ASHRAE) recently incorporated air cleaning devices in their measure of *equivalent clean airflow* when risk of disease transmission is high (e.g. during an epidemic) (ASHRAE 2023).

In this paper, we introduce a spatially local ventilation model to the methodology of Lau *et al.* (2022). While all ventilation systems (including doors, windows and AC units) have local effects, we are motivated by common air purifier designs and introduce a cylindrical device that draws air in through the top and expels clean air from the bottom. This device will be an addition to the existing inbuilt AC system.

The paper is organised as follows. The modelling framework, incorporating a local ventilation system, is presented in §2. In §3, we compare the average aerosol concentration in the room predicted by the local and global ventilation models. In §4 we consider the infection risk to individuals at specific locations and compare the ventilation models. Conclusions and suggestions for future work are provided in §5.

## 2. Modelling framework

### 2.1. Advection–diffusion–reaction (ADR) equation

Consider a 3-dimensional (3D) room with dimensions  $L_x$ ,  $L_y$ ,  $L_z$ , as depicted in figure 1(a). Following Lau *et al.* (2022), we assume a recirculating flow produced by a single AC vent along the top corner and introduce the arclength coordinate  $\xi$ , which follows the recirculating loop. The distance between the recirculation layers is  $L_z/2$  (van Hooff *et al.* 2013) and the total arclength is  $2L_x$ . A cylindrical local ventilation system with radius  $r$  is introduced, which extends over both recirculating layers: Air is drawn into an inlet in the upper layer and expelled from an outlet in the lower layer. We will refer to this device as a *purifier*.

Figure 1(b) shows the computational domain  $(\xi, y)$ . The left/right halves correspond to the upper/lower layers and the purifier inlet and outlet appear as circles removed from the

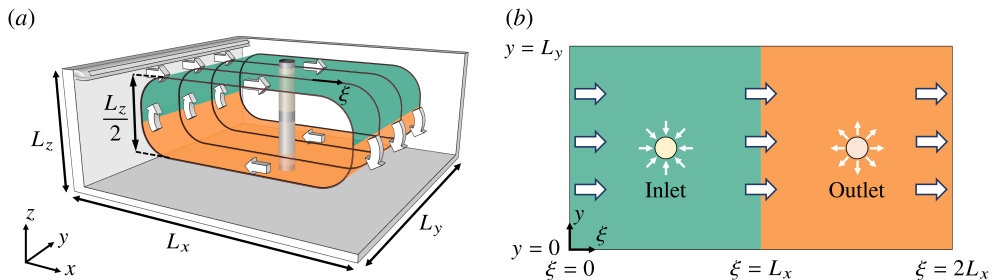


Figure 1: A 3D room with dimensions  $L_x, L_y, L_z$  is shown in (a). A cylindrical local ventilation system crosses the two recirculating layers and the arclength coordinate  $\xi$  follows the recirculating loop. The computational domain  $(\xi, y)$  is shown in (b).

domain, with boundaries

$$\partial_{\text{in}} = \{(\xi, y) : |(\xi, y) - (x_p, y_p)| = r\}, \quad \partial_{\text{out}} = \{(\xi, y) : |(\xi, y) - (2L_x - x_p, y_p)| = r\}, \quad (2.1a,b)$$

where  $(x_p, y_p)$  denotes the location of the purifier in the  $(x, y)$ -plane, and we will assume throughout this work that the purifier is in the centre of the room. Although the purifier design is motivated by real-life devices (Dbouk *et al.* 2021), in this quasi-3D model the device extends the entire height of the room, which is significantly taller than real-life purifiers. However, this simplification allows for a direct comparison with the model of Lau *et al.* (2022) while still offering useful and practical insights.

Consider a single infectious individual standing at  $\mathbf{x}_0 = (x_0, y_0)$  and talking continuously. Talking produces around 10 times as many aerosols as breathing (Asadi *et al.* 2019): a reasonable worst-case scenario for an asymptomatic person. We assume, as in Lau *et al.* (2022), that the concentration of aerosols,  $C(\xi, y, t)$ , is governed by the ADR equation

$$\frac{\partial C}{\partial t} + \nabla \cdot (\mathbf{v}C) - \nabla \cdot (K\nabla C) = R\delta(\xi - x_0)\delta(y - y_0) - (\lambda + \beta + \sigma)C, \quad (2.2)$$

where  $\mathbf{v} = (u, v)$  is a vector field describing the airflow around the recirculating loop;  $K$  is the eddy diffusion coefficient;  $R$  is the (constant) aerosol production rate; and  $\lambda, \beta, \sigma$  are global removal rates due to ventilation, biological deactivation, and gravitational settling, respectively. Parameter values are given in table 1; more details are provided in Lau *et al.* (2022).

The recirculating loop is central to the modelling framework so the AC must be switched on. Following Lau *et al.* (2022), we model this inbuilt ventilation with the global removal term  $\lambda$  and set an air-exchange rate of 0.72 air changes per hour (ACH): the ‘poor ventilation’ scenario of Lau *et al.* (2022) (from classroom data, Guo *et al.* 2008). This reflects a broken or poorly maintained AC system that moves air around but is ineffective at removing aerosols.

Aerosol production begins at  $t = 0$ , so we set the initial condition  $C(\xi, y, 0) = 0$ . Periodic conditions across the left and right boundaries ( $\xi = 0, 2L_x$ ) complete the recirculating loop,

$$C(0, y, t) = C(2L_x, y, t), \quad \frac{\partial C}{\partial \xi}(0, y, t) = \frac{\partial C}{\partial \xi}(2L_x, y, t), \quad (2.3a,b)$$

and there is no flux through the walls at  $y = 0, L_y$ ,

$$\frac{\partial C}{\partial y}(\xi, 0, t) = \frac{\partial C}{\partial y}(\xi, L_y, t) = 0. \quad (2.4)$$

At the purifier inlet, aerosols are carried out of the domain by advection (no diffusive flux),

Parameter	Symbol	Value	Source
Room length	$L_x$	8 m	Lau <i>et al.</i> (2022)
Room width	$L_y$	8 m	Lau <i>et al.</i> (2022)
Room height	$L_z$	3 m	Lau <i>et al.</i> (2022)
Room volume	$V$	192 m <sup>3</sup>	$L_x \times L_y \times L_z$
AC airflow speed	$u_0$	0.15 ms <sup>-1</sup>	(ASHRAE 2020)
Aerosol emission rate (talking)	$R$	5 aerosols/s	(Lau <i>et al.</i> 2022)
Virus deactivation rate	$\beta$	$1.7 \times 10^{-4} \text{ s}^{-1}$	(van Doremalen 2020)
Gravitational settling rate	$\sigma$	$1.1 \times 10^{-4} \text{ s}^{-1}$	(De Oliveira <i>et al.</i> 2021)
Air-exchange rate	$\lambda$	0.72 ACH: $2 \times 10^{-4} \text{ s}^{-1}$ 1.4 ACH: $4.0 \times 10^{-4} \text{ s}^{-1}$ 6 ACH: $1.7 \times 10^{-3} \text{ s}^{-1}$	(Guo <i>et al.</i> 2008) see table 2 see table 2
Eddy diffusion coefficient	$K$	0.72 ACH: $5.3 \times 10^{-3} \text{ m}^2 \text{ s}^{-1}$ 1.4 ACH: $1.0 \times 10^{-2} \text{ m}^2 \text{ s}^{-1}$ 6 ACH: $4.5 \times 10^{-2} \text{ m}^2 \text{ s}^{-1}$	(Foat <i>et al.</i> 2020), (2.6) (Foat <i>et al.</i> 2020), (2.6) (Foat <i>et al.</i> 2020), (2.6)
Breathing rate	$\rho$	$1.3 \times 10^{-4} \text{ m}^3 \text{ s}^{-1}$	(Hallett <i>et al.</i> 2020)
Infectivity constant	$I$	0.0069	(Lau <i>et al.</i> 2022)
Location of purifier centre	$(x_p, y_p)$	(4,4) m	Room centre: $(L_x/2, L_y/2)$
Radius of purifier	$r$	0.1 m	

Table 1: Parameters and their values.

and no aerosols enter the domain at the outlet (no total flux),

$$\hat{\mathbf{n}} \cdot (K\nabla C) = 0 \text{ on } \partial_{\text{in}}, \quad \hat{\mathbf{n}} \cdot (\mathbf{v}C - K\nabla C) = 0 \text{ on } \partial_{\text{out}}, \quad (2.5a,b)$$

where  $\hat{\mathbf{n}}$  denotes the unit vector normal to each boundary, directed out of the domain.

It is unclear from the methodology of Foat *et al.* (2020) how to determine an eddy diffusion coefficient  $K$  for this scenario since the AC vent and purifier outlet have different surface areas. We assume that  $K$  is related to the total air-exchange rate as follows,

$$K = (\lambda + \lambda_p) \sqrt[3]{\frac{V^2}{2}}, \quad (2.6)$$

where  $\lambda_p$  is the air-exchange rate of the purifier (discussed below), so that the value of  $K$  is the same for equivalent global and local ventilation levels.

Following Lau *et al.* (2022), we assume that the majority of aerosols remain within the recirculating loop and are well-mixed over this height. Hence, the concentration in aerosols/m<sup>3</sup> is given by

$$C(x, y, t) = \frac{C(\xi = x, y, t) + C(\xi = 2L_x - x, y, t)}{L_z/2}. \quad (2.7)$$

The risk of infection to a susceptible person at any  $(x, y)$  is then calculated using

$$P(x, y, t) = 1 - \exp \left[ -I \int_0^t \rho C(x, y, \tau) d\tau \right], \quad (2.8)$$

where  $I$  is the infectivity constant of the virus and  $\rho$  is the breathing rate (see table 1).

## 2.2. Airflow simulations

In Lau *et al.* (2022), aerosols are advected around the recirculating loop at constant speed  $u_0$  (table 1). Here, we assume that the recirculating loop remains coherent in the presence of a

Parameter	Symbol	Weak purifier	Strong purifier	Source
Flow-rate (CADR)	$Q$	$0.039 \text{ m}^3\text{s}^{-1}$ ( $140 \text{ m}^3\text{h}^{-1}$ )	$0.28 \text{ m}^3\text{s}^{-1}$ ( $1000 \text{ m}^3\text{h}^{-1}$ )	*
Air velocity into purifier	$v_p$	$0.04 \text{ ms}^{-1}$	$0.3 \text{ ms}^{-1}$	(2.13)
Purifier air-exchange rate	$\lambda_p$	$2.0 \times 10^{-4} \text{ s}^{-1}$	$1.5 \times 10^{-3} \text{ s}^{-1}$	$Q/V$
Total air-exchange rate	$\lambda_{\text{tot}}$	$4.0 \times 10^{-4} \text{ s}^{-1}$	$1.7 \times 10^{-3} \text{ s}^{-1}$	$\lambda + \lambda_p$
Equivalent global ACH		1.4 ACH	6 ACH	$3600\lambda_{\text{tot}}$

Table 2: Parameters for the two purifier settings with  $\lambda = 2 \times 10^{-4} \text{ s}^{-1}$  (0.72 ACH).

\* Weak purifier: Dbouk *et al.* (2021), Strong purifier: Kähler *et al.* (2020).

purifier, leading to a modified  $\mathbf{v} = (u, v)$  such that air enters and leaves the purifier with a specified constant speed  $v_p$ ,

$$\mathbf{v} \cdot \hat{\mathbf{n}} = v_p \text{ on } \partial_{\text{in}}, \quad \mathbf{v} \cdot \hat{\mathbf{n}} = -v_p \text{ on } \partial_{\text{out}}. \quad (2.9a,b)$$

We also require that  $\mathbf{v}$  satisfies the periodic boundary condition

$$\mathbf{v}(0, y) = \mathbf{v}(2L_x, y). \quad (2.10)$$

A vector field that satisfies (2.9) and (2.10) is determined using the Shear Stress Transport (SST) turbulent flow solver (Menter 1994) in COMSOL (a laminar flow solver is not suitable since  $Re > 10\,000$ ). The resulting 2D flow in the  $(\xi, y)$ -plane does not account for the inherently 3D structure of turbulent flow. However, the spreading of aerosols by small-scale turbulent eddies is accounted for by the eddy diffusion coefficient  $K$ .

Imposing no-slip and no-penetration conditions at the walls,

$$\mathbf{v}(\xi, 0) = \mathbf{v}(\xi, L_y) = (0, 0), \quad (2.11)$$

we run the SST solver until a steady-state is reached. This steady velocity,  $\mathbf{v}$ , is then used in the ADR equation (2.2). The results are compared against those of Lau *et al.* (2022) for: (i) no purifier, (ii) a switched off purifier ( $v_p = 0$ ). There is good agreement provided

$$\max_y u(\xi = 0, y) = u_0, \quad (2.12)$$

which is imposed by setting a suitable pressure gradient over the periodic boundaries. Several turbulent models were compared and all resulted in a similar concentration distribution  $C$ .

Two purifier settings are considered based on the clean air delivery rate (CADR) of purifiers used in experimental and computational studies. We define a *weak purifier* with a CADR of  $140 \text{ m}^3\text{h}^{-1}$ , representative of devices for small spaces such as domestic rooms (Dbouk *et al.* 2021) and individual offices; and a *strong purifier* with a CADR of  $1000 \text{ m}^3\text{h}^{-1}$ , representative of devices for larger spaces such as classrooms (Kähler *et al.* 2020) and open-plan offices.

Let  $Q$  denote the flow-rate through the device in  $\text{m}^3\text{s}^{-1}$ . The CADR (stated in  $\text{m}^3\text{h}^{-1}$  by convention) is given by  $\eta Q$  where  $\eta$  is the filter efficacy. We assume that 100% of the aerosols that enter the purifier are trapped by the filter, so  $\eta = 1$  and the CADR and flow-rate  $Q$  are thus equivalent. For a cylindrical purifier (circumference  $2\pi r$ ) with an inlet half the height of the room ( $L_z/2$ ),

$$Q = \pi r L_z v_p. \quad (2.13)$$

We hence compute the velocity  $v_p = Q/(\pi r L_z)$  for a given  $Q$  (see table 2).

Each purifier is compared with an equivalent increase in the global removal term  $\lambda$ . The air-exchange rate associated with each purifier is given by  $\lambda_p = Q/V$ , which we add to the global

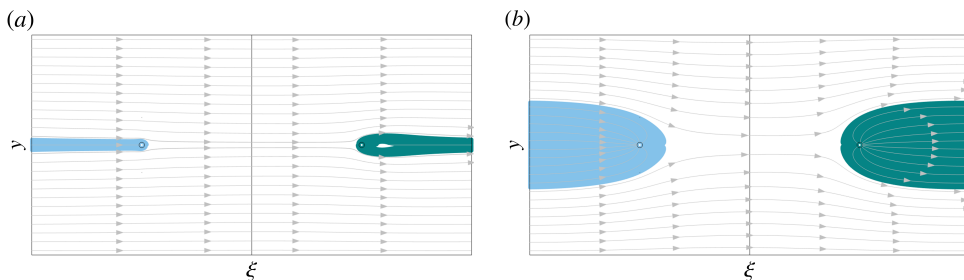


Figure 2: The airflow streamlines in the  $(\xi, y)$ -plane are shown for (a) the weak purifier ( $v_p = 0.04$ ) and (b) the strong purifier ( $v_p = 0.3$ ). The shaded regions indicate streamlines that pass through the purifier inlet (left) and the purifier outlet (right).

removal rate of the AC unit (0.72 ACH) to determine a total air-exchange rate,  $\lambda_{\text{tot}} = \lambda + \lambda_p$  (see table 2). The weak purifier doubles the total air-exchange to 1.4 ACH, less than half the recommended ventilation for classrooms (3 ACH for 30 occupants: Lau *et al.* 2022; ASHRAE 2022). The total air-exchange rate for the strong purifier is 6 ACH, exceeding this recommendation and also sufficient to meet the guidelines for times of heightened infection risk provided the number of occupants is halved (ASHRAE 2023). Hereon in, we will refer to the global ventilation model by the ACH and local ventilation model by the purifier strength.

The streamlines of the airflow  $\mathbf{v}$  are shown in figure 2 for both purifiers. The flow is broadly unidirectional for the weak purifier (figure 2a). Regions in which the streamlines are directed into or out of the purifier are shaded and have a greater area for the strong purifier (figure 2b). In both cases, these regions meet at the periodic boundary.

### 2.3. Computational speed

For each airflow simulation (no purifier, weak purifier, strong purifier) to reach a steady state, computation takes approximately 10 minutes. For the ADR equation (2.2), an event of 4 hours takes around 5 minutes to run, including calculation of the infection risk (2.8). At these computational speeds, advice and guidance can be quickly updated with new information during a fast-changing epidemic. Simulations were performed on a Lenovo IdeaPad Flex 5 laptop, with a 1.3 GHz 4-core Intel Core i7-1065G7 processor and 8 GB of RAM.

## 3. Average aerosol concentration

We define the average aerosol concentration in the room as

$$\bar{C}(t) = \frac{1}{V} \iint_{\Omega} C(\xi, y, t) d\xi dy, \quad (3.1)$$

where  $\Omega$  denotes the computational domain depicted in figure 1(b). Taking appropriate integrals of (2.2) and applying the divergence theorem gives

$$\frac{\partial \bar{C}}{\partial t} = \frac{R}{V} - (\lambda + \beta + \sigma)\bar{C} - \frac{1}{V} \oint_{\partial_{\text{in}}} v_p C dl. \quad (3.2)$$

When  $v_p \neq 0$ , the boundary integral (describing aerosol removal by the purifier) depends on the values of  $C$  on the purifier inlet boundary  $\partial_{\text{in}}$  (2.1). Hence,  $\bar{C}$  depends on the location of the infectious source  $\mathbf{x}_0$  and the vector field  $\mathbf{v}$ . When  $v_p = 0$  there is no local ventilation (as in Lau *et al.* 2022), the boundary integral vanishes, and (3.2) is equivalent to the Wells–Riley

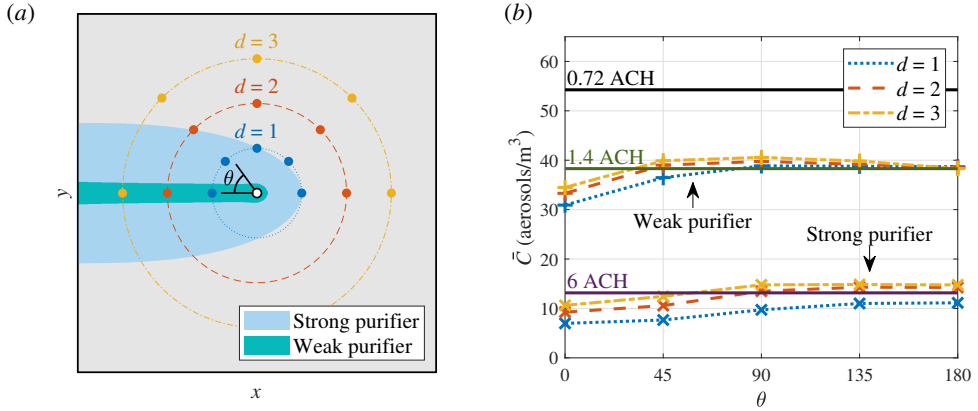


Figure 3: The infectious source locations,  $\mathbf{x}_0$  (3.4), are depicted by filled circles in (a) and the regions where all streamlines are directed into the purifier inlet (figure 2) are shaded for each purifier. For these  $\mathbf{x}_0$ , the average aerosol concentration,  $\bar{C}$  (3.1), after 4 hours is shown for the weak (+) and the strong (x) purifiers in (b). The global ventilation cases are also shown in (b), depicted as horizontal lines (labelled with the ACH).

model used in Miller (2021). In this case the solution to (3.2) is given by

$$\bar{C}(t) = C^* \left[ 1 - e^{-(\lambda + \beta + \sigma)t} \right], \quad \text{where } C^* = \frac{R}{(\lambda + \beta + \sigma)V}. \quad (3.3)$$

Hence,  $\bar{C}$  does not depend on  $\mathbf{x}_0$  or  $\mathbf{v}$  for the global ventilation cases, and  $\bar{C} \rightarrow C^*$  as  $t \rightarrow \infty$ .

We express the location of the infectious source relative to the purifier location as

$$\mathbf{x}_0 = (x_0, y_0) = (x_p - d \cos \theta, y_p + d \sin \theta), \quad (3.4)$$

where  $d$  is the distance from the purifier and  $\theta$  is the angle (in degrees) from the line  $y = L_y/2$ . The problem is symmetric in this line so we consider only  $\theta \in [0, 180]$ . Figure 3(a) shows all choices of  $(d, \theta)$  considered here.

To compare the long-time behaviour of the different ventilation models,  $\bar{C}$  is depicted in figure 3(b) after an event of 4 hours, ensuring  $C$  reaches a steady-state in every case. For the global ventilation models,  $\bar{C}$  is depicted by horizontal lines, which agree with  $C^*$  (3.3). For most  $(d, \theta)$  choices, there is good agreement between each purifier and the equivalent global ventilation. For the weak purifier, the only significant deviation is when  $\theta = 0$  (for all values of  $d$ ). For the strong purifier, the discrepancy is significant for  $d = 1$  (for all values of  $\theta$ ) and for small  $\theta$  when  $d = 2, 3$ . Where the results differ the most, global ventilation predicts a greater  $\bar{C}$  than the equivalent local ventilation. When  $d = 2, 3$ , the global ventilation model predicts a larger  $\bar{C}$  than the purifiers for some  $\theta$ , but the discrepancy is relatively small.

Figure 3(b) shows that  $\bar{C}$  increases with distance from the purifier  $d$ , but there is also dependence on  $\theta$  that is related to the streamlines of  $\mathbf{v}$ . The regions where the streamlines enter each purifier are shaded in figure 3(a), and  $\bar{C}$  is notably lower when  $\mathbf{x}_0$  is within (or close to) these regions. For values of  $\mathbf{x}_0$  outside these regions, there is less variation in  $\bar{C}$  and closer agreement with the equivalent global ventilation.

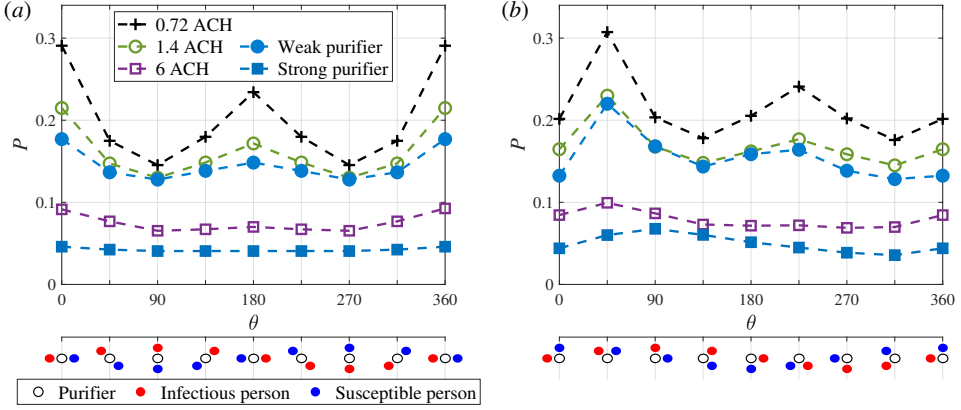


Figure 4: The infection risk,  $P$  (2.8), after 1 hour to the susceptible person (a) opposite ( $\phi = 180$ ) and (b) left ( $\phi = 90$ ) of the infectious person (4.1). Global ventilation cases are labelled with the ACH (open symbols) and the equivalent local ventilation (purifier) is depicted by filled symbols of the same shape. Schematics in the lower axes depict the scenario for each  $\theta$ .

#### 4. Infection risk to susceptible people nearby

Our spatially varying ADR model allows us to determine the infection risk to susceptible people at specific locations (2.8). We express the location of a susceptible person  $\mathbf{x}_s$  as

$$\mathbf{x}_s = (x_s, y_s) = (x_p - d_s \cos(\theta + \phi), y_p + d_s \sin(\theta + \phi)), \quad (4.1)$$

where  $\phi$  is the angle between  $\mathbf{x}_0$  and  $\mathbf{x}_s$ , and  $d_s$  is the distance from the purifier. We consider a susceptible person directly opposite the infectious person,  $\phi = 180$ , and a susceptible person left of the infectious person,  $\phi = 90$  (depicted in figure 4). We restrict interest to  $d = 1$ , the case with the greatest discrepancy between the local and global ventilation models in figure 3. To reflect a scenario in which individuals are in close proximity, we also set  $d_s = 1$ . This is reflective of classrooms, restaurants, galleries and other social events, with 1 hour being a representative event duration. However, in reality, these purifiers are potentially too large and noisy for use in such a setting.

Figure 4 shows the infection risk to susceptible people opposite and left of the infectious person after 1 hour, with the scenario for each  $\theta$  depicted on the lower axes. Figure 4(a) is symmetric around  $\theta = 180$  because the problem is symmetric in the line  $y = L_y/2$ . Moreover, the infection risk to a susceptible person right of the infectious person ( $\phi = -90$ ) can be deduce from figure 4(b) by reflection in this line ( $\theta \rightarrow 360 - \theta$ ).

After 1 hour, the infection risk is below 40% in all cases and the infection risk is lower with the purifiers than with the equivalent global ventilation. The weak purifier has had only a marginal effect when compared against the baseline example of 0.72 ACH, and shows close agreement with the corresponding global ventilation of 1.4 ACH. The infection risk is lower for the strong purifier than for the equivalent global ventilation of 6 ACH for all values of  $\theta$ . The greatest discrepancy is when  $\theta = 0$ , with the strong purifier predicting half the infection risk of the 6 ACH global ventilation (figure 4a,b).

The streamlines of  $\mathbf{v}$  again provide insight into these results. For the global ventilation models and the weak purifier, peaks occur when  $y_0 = y_s$  due to the broadly unidirectional flow around the recirculating loop, with lower peaks when the aerosols travel further (e.g.  $\theta = 180$  in figure 4a). For the strong purifier, the largest infection risk ( $\theta = 90$  in figure 4b)

corresponds to the susceptible person being directly downstream from the infectious person according to the significantly modified streamlines in this case (figure 2b).

Under the WMR assumption, the infection risk is calculated based on the average aerosol concentration  $\bar{C}$  (3.3). This approach predicts the following infection risks: 8.8% for 0.72 ACH, 7.5% for 1.4 ACH, and 3.6% for 6 ACH. This is a significant underestimate compared to the corresponding values in figure 4 since the close proximity to the infectious source results in a concentration significantly greater than the room average at all times.

## 5. Summary and conclusions

The recent ADR model for airborne virus transmission (Lau *et al.* 2022) was modified to incorporate a local ventilation system motivated by air purifiers. A weak purifier (CADR = 140 m<sup>3</sup>h<sup>-1</sup>) and a strong purifier (CADR = 1000 m<sup>3</sup>h<sup>-1</sup>) were compared against equivalent increases in the global ventilation (1.4 ACH and 6 ACH, respectively).

For each purifier, the average aerosol concentration after reaching a steady-state was compared against the equivalent global ventilation, with good agreement in most cases (figure 3). The infection risk to susceptible people near to the purifier after 1 hour was also considered: The weak purifier showed close agreement with the global ventilation model, whereas the strong purifier predicted a lower infection risk than the equivalent global ventilation (figure 4). The largest discrepancies between the local and global ventilation models were observed when the infectious person was located inside or near to the regions where the airflow streamlines are directed into the purifier inlet (figure 2).

When modelling airborne transmission, Wells–Riley models (e.g. Miller 2021) offer great computational speed but are highly simplistic, whereas CFD models (particularly those that track individual particles, e.g. Dbouk *et al.* 2021) provide significant detail at great computational expense. The ADR model of Lau *et al.* (2022) offers a compromise, with greater detail than Wells–Riley models (spatial variation) at low computational cost. By adding further complexity to the problem, the present model is able to explore the effects of local ventilation over hours, the time-frame over which airborne transmission occurs, while retaining relatively small computational times.

In future, this computational speed could facilitate a more thorough investigation of the problem, exploring factors such as the purifier location, size, and strength. The model could be further developed by incorporating a spatially varying eddy diffusion coefficient or an unsteady airflow. Building on this work, the local ventilation effects of air-conditioning, windows, doors, and other purifier designs could be explored in a similar manner.

**Acknowledgements.** The authors wish to acknowledge the contributions of Dr. Aaron English, Dr. Raquel González Fariña and Dr. Attila Kovács. We are grateful to Siân Grant for generating Figure 1(a).

**Funding.** A.P. and K.K. gratefully acknowledge funding from a Sêr Cymru ‘Tackling COVID-19’ grant, awarded by the Welsh Government. I.M.G. is grateful to the Royal Society for funding through a University Research Fellowship.

**Declaration of interests.** The authors report no conflict of interest.

## REFERENCES

- ASADI, S., WEXLER, A. S., CAPP, C. D., BARREDA, S., BOUVIER, N. M. & RISTENPART, W. D. 2019 Aerosol emission and superemission during human speech increase with voice loudness. *Scientific Reports* **9** (1), 1–10.
- ASHRAE 2020 Standard 55-2020, Thermal environmental conditions for human occupancy.
- ASHRAE 2022 Standard 62.1-2022, Ventilation and acceptable indoor air quality.
- ASHRAE 2023 Standard 241-2023, Control of infectious aerosols.

- BUONANNO, G., STABILE, L. & MORAWSKA, L. 2020 Estimation of airborne viral emission: Quanta emission rate of SARS-CoV-2 for infection risk assessment. *Environ. Int.* **141**, 105794.
- BURGMANN, S. & JANOSKE, U. 2021 Transmission and reduction of aerosols in classrooms using air purifier systems. *Phys. Fluids* **33**, 033321.
- DAI, H. & ZHAO, B. 2020 Association of the infection probability of COVID-19 with ventilation rates in confined spaces. *Build Sim.* **13**(6), 1321–1327.
- DBOUK, T., ROGER, F. & DRIKAKIS, D. 2021 Reducing indoor virus transmission using air purifiers. *Phys. Fluids* **33** (10), 103301.
- DE OLIVEIRA, P. M., MESQUITA, L. C. C., GKANTONAS, S., GIUSTI, A. & MASTORAKOS, E. 2021 Evolution of spray and aerosol from respiratory releases: Theoretical estimates for insight on viral transmission. *Proc. Math. Phys. Eng. Sci.* **477** (2245), 20200584.
- VAN DOREMALEN, N. ET AL. 2020 Aerosol and surface stability of SARS-CoV-2 as compared with SARS-CoV-1. *N. Engl. J. Med.* **382** (16), 1564–1567.
- FOAT, T., DRODGE, J., NALLY, J. & PARKER, S. 2020 A relationship for the diffusion coefficient in eddy diffusion based indoor dispersion modelling. *Build Environ.* **169**, 106591.
- GÜNTHER, T. ET AL. 2020 SARS-CoV-2 outbreak investigation in a German meat processing plant. *EMBO Mol. Med.* **12**, e13296.
- GUO, H., MORAWSKA, L., HE, C. & GILBERT, D. 2008 Impact of ventilation scenario on air exchange rates and on indoor particle number concentrations in an air-conditioned classroom. *Atmos. Environ.* **42** (4), 757–768.
- HALLETT, S., TORO, F. & ASHURST, J. V. 2020 Physiology, tidal volume. [Updated 2020 Jun 1]. In: StatPearls [Internet]. Treasure Island (FL): StatPearls Publishing; 2020 Jan-. Available from: <https://www.ncbi.nlm.nih.gov/books/NBK482502/>.
- HO, C. K. 2021 Modelling airborne transmission and ventilation impacts of a COVID-19 outbreak in a restaurant in Guangzhou, China. *Int J Comput Fluid Dyn.*
- VAN HOOFF, T., BLOCKEN, B. & VAN HEIJST, G. J. F. 2013 On the suitability of steady RANS CFD for forced mixing ventilation at transitional slot Reynolds numbers. *Indoor Air* **23** (3), 236–249.
- KÄHLER, C. J., FUCHS, T. & HAIN, R. 2020 Can mobile indoor air cleaners effectively reduce an indirect risk of SARS-CoV-2 infection by aerosols? *Hg. v. Universität der Bundeswehr München. Strömungsmechanik und Aerodynamik* **18**.
- LAU, Z., GRIFFITHS, I. M., ENGLISH, A. & KAOURI, K. 2022 Predicting the spatio-temporal infection risk in indoor spaces using an efficient airborne transmission model. *Proc. Math. Phys. Eng. Sci.* **478** (2259), 20210383.
- LELIEVELD, J. ET AL. 2020 Model calculations of aerosol transmission and infection risk of COVID-19 in indoor environments. *Int. J. Environ. Res. Public Health* **17**, 8114.
- MENTER, F. R. 1994 Two-equation eddy-viscosity turbulence models for engineering applications. *AIAA Journal* **32** (8), 1598–1605.
- MILLER, S. L. ET AL. 2021 Transmission of SARS-CoV-2 by inhalation of respiratory aerosol in the Skagit Valley Chorale superspreading event. *Indoor Air* **31**, 314–323.
- MORAWSKA, L. & MILTON, D. K. 2020 It is time to address airborne transmission of COVID-19. *Clin. Infect. Dis.* **6**, ciaa939.
- NARAYANAN, S. R. & YANG, S. 2021 Airborne transmission of virus-laden aerosols inside a music classroom: Effects of portable purifiers and aerosol injection rates. *Phys. Fluids* **33**, 033307.
- NIGHTINGALE, F. 1860 *Notes on Nursing: What it is, and what it is not*. Harrison London.
- RILEY, E. C., MURPHY, G. & RILEY, R. L. 1978 Airborne spread of measles in a suburban elementary school. *Am. J. Epidemiol.* **107**, 421–432.
- SHAFAGHI, A. H., ROKHSAR, F. T. F., KOŞAR, A. & GHORBANI, M. 2020 On the effect of the respiratory droplet generation condition on COVID-19 transmission. *Fluids* **5** (3), 113.
- SHAO, S., ZHOU, D., HE, R., LI, J., ZOU, S., MALLERY, K., KUMAR, S. & YANG, S. 2021 Risk assessment of airborne transmission of COVID-19 by asymptomatic individuals under different practical settings. *J. Aerosol Sci.* **151**, 105661.
- VERNEZ, D., SCHWARZ, S., SAUVAIN, J.-J., PETIGNAT, C. & SUAREZ, G. 2021 Probable aerosol transmission of SARS-CoV-2 in a poorly ventilated courtroom. *Indoor Air* **31** (6), 1776–1785.
- VUORINEN, V. ET AL. 2020 Modelling aerosol transport and virus exposure with numerical simulations in relation to SARS-CoV-2 transmission by inhalation indoors. *Safety Science* **130**, 104866.